2018

Robust memristors based on layered two-dimensional materials

Miao Wang
Nanjing University

Songhua Cai
Nanjing University

Chen Pan
Nanjing University

Chenyu Wang
Nanjing University

Xiaojuan Lian
Nanjing University

See next page for additional authors

Recommended Citation
Wang, Miao; Cai, Songhua; Pan, Chen; Wang, Chenyu; Lian, Xiaojuan; Zhuo, Ye; Xu, Kang; Cao, Tianjun; Pan, Xiaoqing; Wang, Baigeng; Liang, Shi-Jun; Yang, J. Joshua; Wang, Peng; and Miao, Feng, "Robust memristors based on layered two-dimensional materials" (2018). *Nature Electronics*. 1184.
https://doi.org/10.1038/s41928-018-0021-4

ARTICLES
https://doi.org/10.1038/s41928-018-0021-4

nature electronics

Corrected: Author correction

Robust memristors based on layered two-dimensional materials

Miao Wang[1,7], Songhua Cai[2,7], Chen Pan[1], Chenyu Wang[1], Xiaojuan Lian[1], Ye Zhuo[3], Kang Xu[1], Tianjun Cao[1], Xiaoqing Pan[2,4,5], Baigeng Wang[1], Shi-Jun Liang[1], J. Joshua Yang[3*], Peng Wang[2,6*] and Feng Miao[1*]

Van der Waals heterostructures are formed by stacking layers of different two-dimensional materials and offer the possibility to design new materials with atomic-level precision. By combining the valuable properties of different 2D systems, such heterostructures could potentially be used to address existing challenges in the development of electronic devices, particularly those that require vertical multi-layered structures. Here we show that robust memristors with good thermal stability, which is lacking in traditional memristors, can be created from a van der Waals heterostructure composed of graphene/$MoS_{2-x}O_x$/graphene. The devices exhibit excellent switching performance with an endurance of up to 10^7 and a high operating temperature of up to 340 °C. With the help of in situ electron microscopy, we show that the thermal stability is due to the $MoS_{2-x}O_x$ switching layer, as well as the graphene electrodes and the atomically sharp interface between the electrodes and the switching layer. We also show that the devices have a well-defined conduction channel and a switching mechanism that is based on the migration of oxygen ions. Finally, we demonstrate that the memristor devices can be fabricated on a polyimide substrate and exhibit good endurance against over 1,000 bending cycles, illustrating their potential for flexible electronic applications.

Memristors are a leading candidate for future storage and neuromorphic computing technologies[1–10] due to characteristics such as device scalability, multi-state switching, fast switching speed, high switching endurance and CMOS compatibility[6,11–16]. Most research and development efforts have been focused on improving device switching performance in optimal conditions, and the reliability of memristors in harsh environments such as at high temperature and on bending substrates has so far received much less attention. Since the programming processes in memristors based on traditional oxide materials mostly rely on ion moving and ionic valence changing[16,17], the thermal instability at elevated temperatures could result in device failure[18]. Thus, to the best of our knowledge, there has been no reliable switching behaviours observed in memristors at temperatures above 200 °C[18,19], which limits their potential application in harsh electronics such as those demanded in aerospace, military, automobile, geothermal, oil and gas industries. Common high temperature electronic materials, such as SiC and III-nitride[20,21], are not adoptable in fabricating memristors, and therefore searching for new materials and structures for robust memristors with good performance is desirable.

By stacking two-dimensional (2D) layered materials together[22–30], van der Waals (vdW) heterostructures can combine the superior properties of each 2D component. 2D materials have shown excellent structural stability[31,32] and electrical properties, which could provide significant improvements in the robustness of electronic devices. For example, graphene possesses unparalleled breaking strength, and ultra-high thermal and chemical stabilities[33]; molybdenum disulfide (MoS_2) has shown good flexibility, large Young's modulus (comparable to stainless steel),[34] and excellent thermal stability up to 1,100 °C[32]; and various functionalized 2D material layers, or certain grain boundaries within 2D materials, have shown switching behaviours[35–44]. Since both the thickness and roughness of 2D layered materials can be controlled accurately at the atomic scale, the reliability and uniformity of the electronic devices based on such materials and their vdW heterostructures could also be optimized.

In this Article, we report robust memristors based on a vdW heterostructure made of fully layered 2D materials (graphene/$MoS_{2-x}O_x$/graphene), which exhibit repeatable bipolar resistive switching with endurance up to 10^7 and high thermal stability with an operating temperature of up to 340 °C. The $MoS_{2-x}O_x$ layer was found to be responsible for the high thermal stability of the devices by performing high temperature in situ high-resolution transmission electron microscopy (HRTEM) studies. Further in situ scanning transmission electron microscopy (STEM) investigations on the cross section of a functional device revealed a well-defined conduction channel and a switching mechanism based on the migration of oxygen ions. The atomic layered structure of both memristive material ($MoS_{2-x}O_x$) and electrodes (graphene) was found to be well maintained during the switching processes, which plays a crucial role in determining the robustness of the devices. Finally, the mechanical flexibility of such devices was demonstrated on polyimide (PI) substrate with a good endurance against mechanical bending of over 1,000 times.

Device fabrication and switching performance

Figure 1a shows the schematic drawing and the crystal structure of graphene/$MoS_{2-x}O_x$/graphene (GMG) devices. Multi-layer graphene

[1]National Laboratory of Solid State Microstructures, School of Physics, Collaborative Innovation Center of Advanced Microstructures, Nanjing University, Nanjing, China. [2]College of Engineering and Applied Sciences and Collaborative Innovation Center of Advanced Microstructures, Nanjing University, Nanjing, China. [3]Department of Electrical and Computer Engineering, University of Massachusetts, Amherst, MA, USA. [4]Department of Chemical Engineering and Materials Science, University of California, Irvine, CA, USA. [5]Department of Physics and Astronomy, Univeristy of California, Irvine, CA, USA. [6]Center for the Microstructures of Quantum Materials and Research Center for Environmental Nanotechnology, Nanjing University, Nanjing, China. [7]These authors contributed equally: Miao Wang and Songhua Cai. *e-mail: jjyang@umass.edu; wangpeng@nju.edu.cn; miao@nju.edu.cn

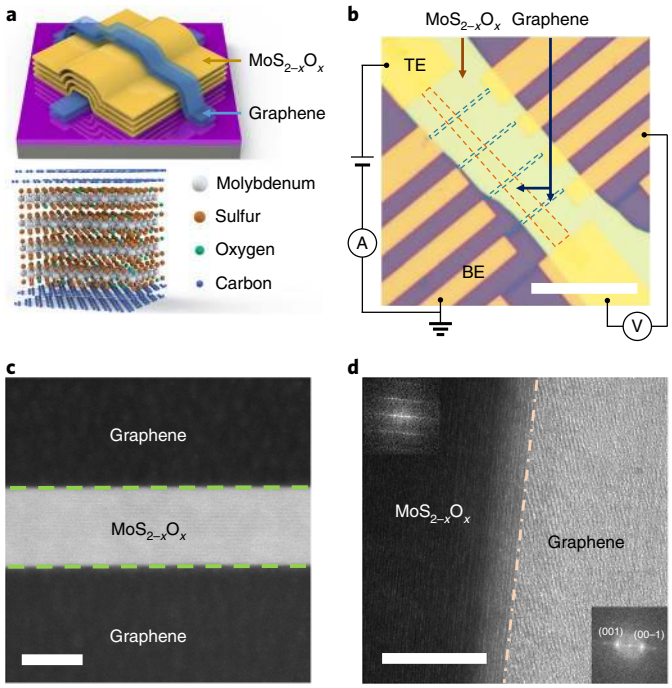

Fig. 1 | GMG devices and cross-section images. a, Top: schematic drawing of the GMG devices. Bottom: crystal structure of the GMG devices. **b**, Optical microscope image and measurement setup of a GMG device. Scale bar, 25 μm. The top (TE) and bottom (BE) graphene electrodes are highlighted by orange and blue dashed boxes, respectively. Four-probe measurements were carried out to rule out the resistance of graphene electrodes. **c**, Cross-section HAADF image of a pristine GMG device. Scale bar, 20 nm. **d**, Cross-section HRTEM image of a pristine GMG device. Top and bottom insets: power spectra of the $MoS_{2-x}O_x$ layer and graphene in the HRTEM image, respectively. $MoS_{2-x}O_x$ maintains layered crystal structure after the oxidization, with excellent contact with graphene. Scale bar, 20 nm.

(~8 nm thick) and MoS_2 (~40 nm thick) membranes were mechanically exfoliated and deposited on SiO_2/Si wafers. We oxidized MoS_2 membranes at 160 °C for 1.5 h in ambient air to obtain the layered $MoS_{2-x}O_x$ membrane, where $x \approx 0.3$ according to Energy Dispersive X-Ray Spectroscopy (EDS) analysis (Fig. 5d). Figure 1b shows the optical image of a typical GMG device and measurement setup. The stacked vdW heterostructure was obtained by using standard polyvinyl alcohol (PVA) transfer method. Figures 1c and 1d show the cross-section high angle annular dark-field (HAADF) and HRTEM images respectively. Remarkably, the $MoS_{2-x}O_x$ layer exhibits excellent layered crystal structure after the oxidization process. Compared to the previous works of replacing either electrode or switching layer by layered materials to improve performance[35–44], one major advantage of our GMG devices based vdW heterostructure is the realization of the atomically sharp interfaces between the switching layer and the electrodes (Fig. 1d). This is not achievable in traditional metal/oxide/metal based memristors fabricated by sputtering and evaporating[16,17]. Since the switching performance of memristors is largely affected by the roughness of the switching interface[5,45], high performance could be expected in the GMG devices.

We then examined the switching performance of our GMG devices by using four-probe electrical measurements (to rule out the line resistance). Figure 2a shows the repeatable bipolar switching curves of a typical GMG device. The switching polarity is determined by the electroforming voltage polarity, i.e. positive/negative electroforming resulting in ON switching with positive/negative bias and OFF switching with negative/positive bias (see Supplementary Fig. 1a and Supplementary Note 1 for more details). Higher ON/OFF ratio can be achieved with higher current compliance for electroforming and set process (Supplementary Fig. 1b). The switching voltage for the first set operation (orange curve in Fig. 2a) is only slightly larger than that of the subsequent normal set operation (blue I-V), suggesting that no dramatic electroforming process is required for device operations. As shown in Fig. 2b, over 2×10^7 switching cycles were observed by applying fixed voltage pulses (1 μs width with + 3.5 V for set and −4.8 V for reset). We also used fixed voltage pulses (+ 3 V for set and −4 V for reset) with progressively broadened width to test the switching speed of our GMG devices. The results show that the GMG device could switch in less than 100 ns and sustain its resistance state under the following wider reading pulses (Fig. 2c). Here we note that this measured switching speed is limited by the parasitic capacitance of the device, not the intrinsic switching speed. In addition, a good retention (~10^5 s) of both ON and OFF states at room temperature was shown in Fig. 2d. During all electrical measurements, the voltages were applied on the graphene top electrode and the graphene bottom electrode was always grounded.

In order to investigate the role of the high-quality interface in the GMG devices, we carried out control experiments by fabricating devices based on Au/$MoS_{2-x}O_x$ (~40 nm)/Au (AMA) structure (using the same $MoS_{2-x}O_x$ membranes as in GMG devices). Repeatable switching behaviours were also observed in AMA devices. We carefully analysed and compared the statistics of the switching parameters in AMA and GMG devices. Compared with the GMG devices, the AMA devices have shown much boarder distributions in both reset and set voltages (see Supplementary Figures 2a–e and Supplementary Note 2), suggesting a larger variance and less reliable resistive switching in AMA devices. A much lower switching endurance with a larger cycle-to-cycle resistance variance was also observed in the AMA devices, as shown in Supplementary Fig. 2f. The cross-section HRTEM studies of an AMA device (see Supplementary Fig. 3 and Supplementary Note 3) revealed a rough interface between the Au electrode and $MoS_{2-x}O_x$ layer, indicating a crucial role possibly played by the high-quality switching interface in memristor devices based on layered materials.

High-temperature performance and thermal stability

To further examine the thermal stability of the GMG devices, we measured their switching performance at elevated temperatures. Various switching curves of a typical GMG device at ambient temperatures ranging from 20 °C to 340 °C are shown in Fig. 3a. The device remained fully functional at 340 °C. We also used voltage pulses (fixed width of 1 μs) to test the switching repeatability of the GMG devices at elevated temperatures. As shown in Fig. 3b, the GMG device exhibits a good cycle to cycle reproducibility and a stable switching window at three chosen temperatures (100 °C, 200 °C and 300 °C). The retention of both ON and OFF states at elevated temperatures was also examined. As shown in Fig. 3c, we observed no significant resistance change of ON/OFF state over an approximately 10^5 s testing time at 160 °C and 340 °C respectively, suggesting a great reliability of the GMG devices at elevated temperatures. The demonstrated operating temperature of 340 °C is record-high for memristors, and much higher than the previously reported highest temperature of 200 °C[19], suggesting potential applications of GMG devices as high-density memory/computing units in future high-temperature harsh electronics.

Compared with the amorphous oxide switching layer used in the traditional memristors, the layered crystal structure of $MoS_{2-x}O_x$ could be responsible for the robustness of GMG devices in terms of high thermal stability. In order to verify this, we performed in situ HRTEM studies on the $MoS_{2-x}O_x$ membranes at high temperatures (Fig. 4a–d). Remarkably, the $MoS_{2-x}O_x$ membrane maintains excellent crystal structure at temperatures up to 800 °C. Ion migration starts to occur only when the temperature increases to 900 °C or

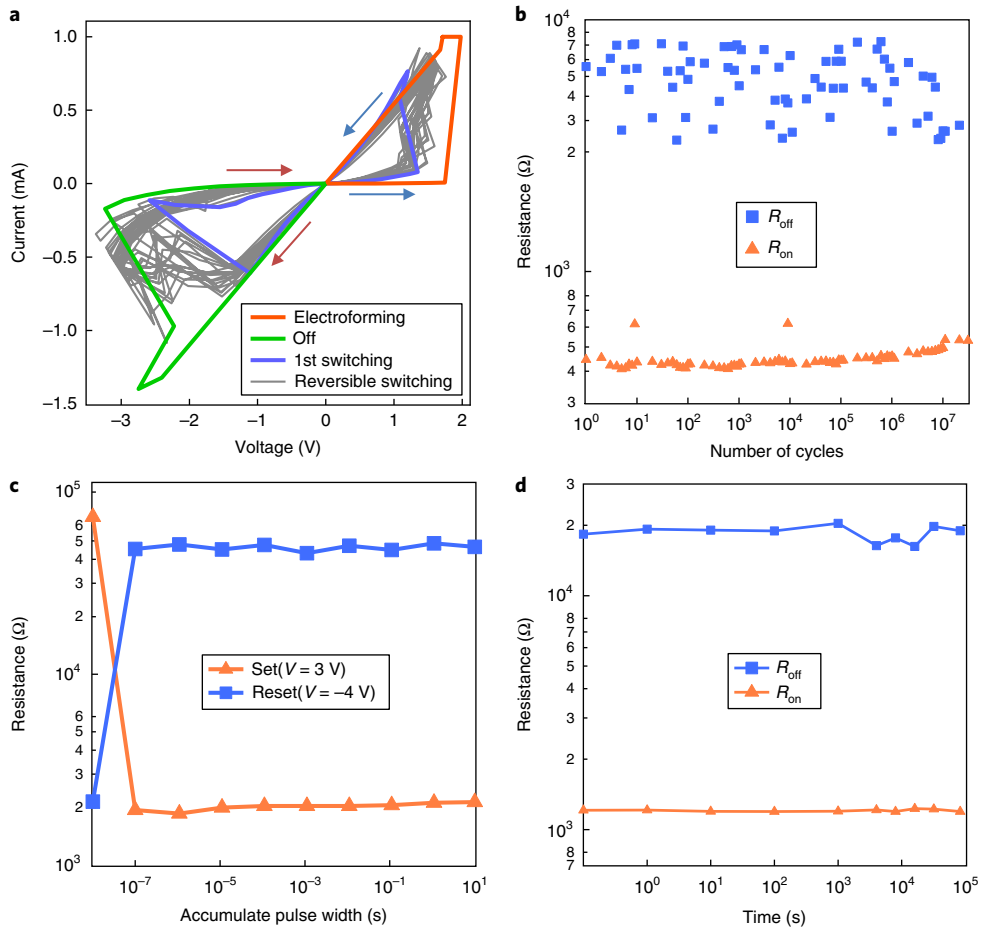

Fig. 2 | Electrical characterizations of the GMG devices. a, DC switching curves of a GMG device with an electroforming current compliance of 1 mA. The green line is the reset process after electroforming step. The arrows indicate the switching directions. **b**, Over 2×10^7 switching cycles obtained with 1-μs width pulses applied (about + 3.5 V and −4.8 V dropped across the device for set and reset, respectively). **c**, Switching speed test of a GMG device. The voltage drop across the device is about + 3 V and −4 V for set and reset, respectively. The device can be switched in less than 100 ns and keep its resistance state with wider pulses applied. **d**, About 10^5 s retention time measured in a GMG device. The blue and orange dots represent OFF and ON state resistances, respectively. The resistance values were read at $V_r = 0.1$ V.

higher (see Supplementary Fig. 5 and Supplementary Note 4). As a matter of fact, pristine MoS_2 stays stable at very high temperatures. For example, MoS_2 can still be used as a lubricant at 1,300 °C[46]. Thus, the superior high thermal stability of the $MoS_{2-x}O_x$ layer should be attributed to the structural stability of MoS_2 (since the $MoS_{2-x}O_x$ layer was obtained by oxidizing MoS_2). Such high thermal stability has not been reported in the amorphous oxides used in traditional memristors (such as in Titanium oxides and Tantalum oxides, with phase transition temperatures at 300 °C[47] and 650 °C[48], respectively). The thermal stability of $MoS_{2-x}O_x$ layer also enables the non-switching regions in the devices to maintain their original state at elevated temperatures, hence ensures the stable switching of the GMG devices.

In situ STEM study and microscopic pictures

In order to further reveal the nature of the robustness of GMG devices, it is essential to acquire the microscopic pictures during the electroforming and switching processes. We fabricated electron-transparent cross-sectional TEM samples with a similar GMG structure (Pt/graphene/$MoS_{2-x}O_x$/graphene/conductive silicon substrate, see details in methods section), followed by in situ STEM experiments. This makes it feasible for real-time observation of any voltage-induced structural change, particularly in the conduction channel region, with typical HAADF-STEM and EDS results of different states shown in Fig. 5a–c (pristine, ON and OFF states respectively). The whole area of the cross-sectional device was investigated during the in situ STEM experiment to confirm that there is no region that is critical for the switching except the one shown in Fig. 5. After the electroforming with a positive staircase sweep voltage (from 0 to + 4.5 V) applied on the top electrode (Pt), a dark-contrast region in the $MoS_{2-x}O_x$ layer appeared (in the ON state, shown in Fig. 5b) and barely changed when the device was switched to the OFF state (Fig. 5c). This observation suggests that a conduction channel was formed with some noticeable composition change, as the intensity of the HAADF image is monotonically proportional to atomic number Z[49]. In addition, EDS line-scan analysis was employed to study the elemental composition variations of the $MoS_{2-x}O_x$ layer for three different states as shown in Fig. 5d–f respectively (the scanning directions are indicated by the green arrows in Fig. 5a–c). In the pristine state, the $MoS_{2-x}O_x$ layer shows a uniform atom distribution in stoichiometric proportions with an averaged atomic ratio of molybdenum to sulfur and oxygen at approximate 0.5 (Mo:(S + O) ≈ 1:2, as shown in Fig. 5d and Supplementary Fig. 6). This suggests that sulfur vacancies in $MoS_{2-x}O_x$ could be mostly occupied by oxygen after the thermal oxidation (as schematically shown in Fig. 5g). After the electroforming, a clear reduction of the S atom percentage in the channel region was observed with the atomic ratio of Mo:(S + O) decreased

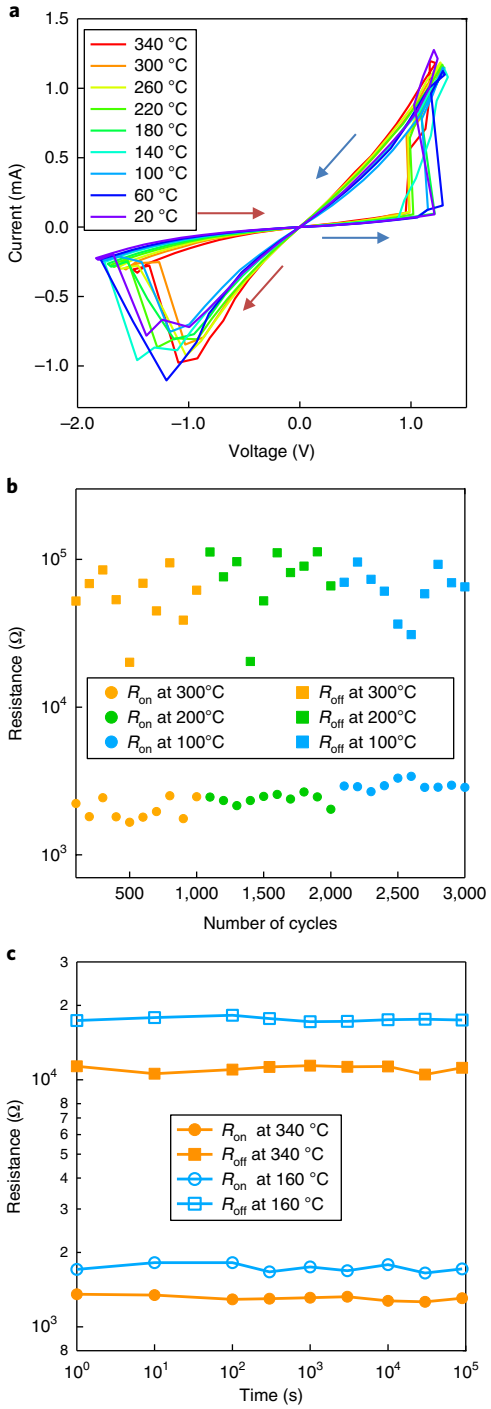

Fig. 3 | Electrical characterizations of the GMG devices at elevated temperatures. a, Switching curves of a GMG device at different temperatures. The arrows indicate the switching directions. The GMG device was able to operate at a high temperature up to 340 °C, demonstrating high thermal stability. **b**, 1,000-time endurance test under 1 µs pulse at 300 °C (orange), 200 °C (green) and 100 °C (blue), respectively. **c**, Retention time at 340 °C (orange) and 160 °C (blue). The resistance values were read at $V_r = 0.1$ V. The good endurance and retention time further demonstrate the high thermal stability of the GMG devices.

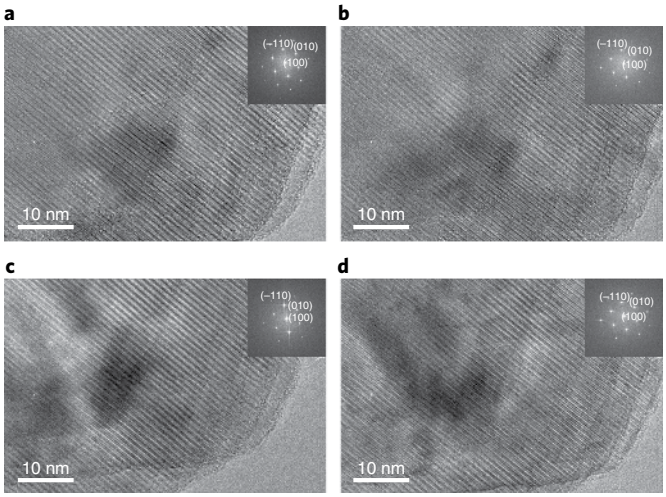

Fig. 4 | In situ HRTEM observation of $MoS_{2-x}O_x$ at elevated temperatures. **a**–**d**, HRTEM images of the same $MoS_{2-x}O_x$ membrane at room temperature (**a**), 300 °C (**b**), 600 °C (**c**) and 800 °C (**d**). $MoS_{2-x}O_x$ maintains excellent crystal structure at 800 °C. Insets: power spectra of the corresponding HRTEM images of the $MoS_{2-x}O_x$ membrane at different temperatures, all of which show the reflections corresponding to the $MoS_{2-x}O_x$ structure. The lattice constant of the $MoS_{2-x}O_x$ membrane is 3.16 Å at 20 °C and 3.19 Å at 800 °C as calculated from the power spectrum images. All images were taken after the target temperatures were kept stable for 10 min.

to approximate 1:1.2, as shown in Fig. 5e. This observation is consistent with the reduced contrast at the channel region in its corresponding HAADF image (Fig. 5b). The loss of S atoms (forming S vacancies) could result from thermophoresis effect due to the Joule heating: the temperature gradient caused by the increasing current drives the lighter ions away from the channel region (as schematically shown in Fig. 5g,h).

Furthermore, a comparison of in situ STEM results between the ON and OFF states could reveal a switching mechanism of GMG devices. It can be seen that there was no noticeable change in the $MoS_{2-x}O_x$ layer as shown in the HAADF image (Fig. 5c), suggesting that no intense atomic movement occurred during the reset process. At the same time, the horizontal line-scan exhibits a percentage increase of oxygen atoms in the channel region for the OFF state, with an atomic ratio of Mo:(S + O) changed to be around 1:2. The amount of S in the channel region remains the same or even slightly decreases from the ON state to the OFF state. The experimentally observed increase of oxygen atoms in the channel region indicates that the oxygen ions near the channel region are driven (mainly by thermal dissolution effect) towards the channel to fill the sulfur vacancies, and consequently switch the device to the OFF state (as schematically shown in Fig. 5i). Here the filled oxygen ions are more mobile than the sulfur ions likely due to the lower barrier energy for motion. For the set process, since thermophoresis effect[50,51] would dominate due to the steep radial temperature gradient produced by Joule heating, the oxygen ions are driven out of the channel region. The switching mechanism primarily based on the migration of oxygen ions with minor structure change of the channel region is believed to be a major origin of the observed high switching performance[16].

Based on our results obtained in the in situ STEM experiments, both the graphene electrodes and the $MoS_{2-x}O_x$ switching layer, together with their atomically sharp interfaces, are considered to be responsible for the high thermal stability of the GMG devices. Firstly, we found that the channel region still maintains layered crystal structure after the electrical operations (see the HRTEM image of the in situ planar GMG device in Supplementary Fig. 7b). By considering the aforementioned extra-high thermal stability of the $MoS_{2-x}O_x$ layer, at elevated temperatures, this could effectively avoid the undesirable migration of oxygen and sulfur ions, and prevent possible reactions between the conduction channel and surround-

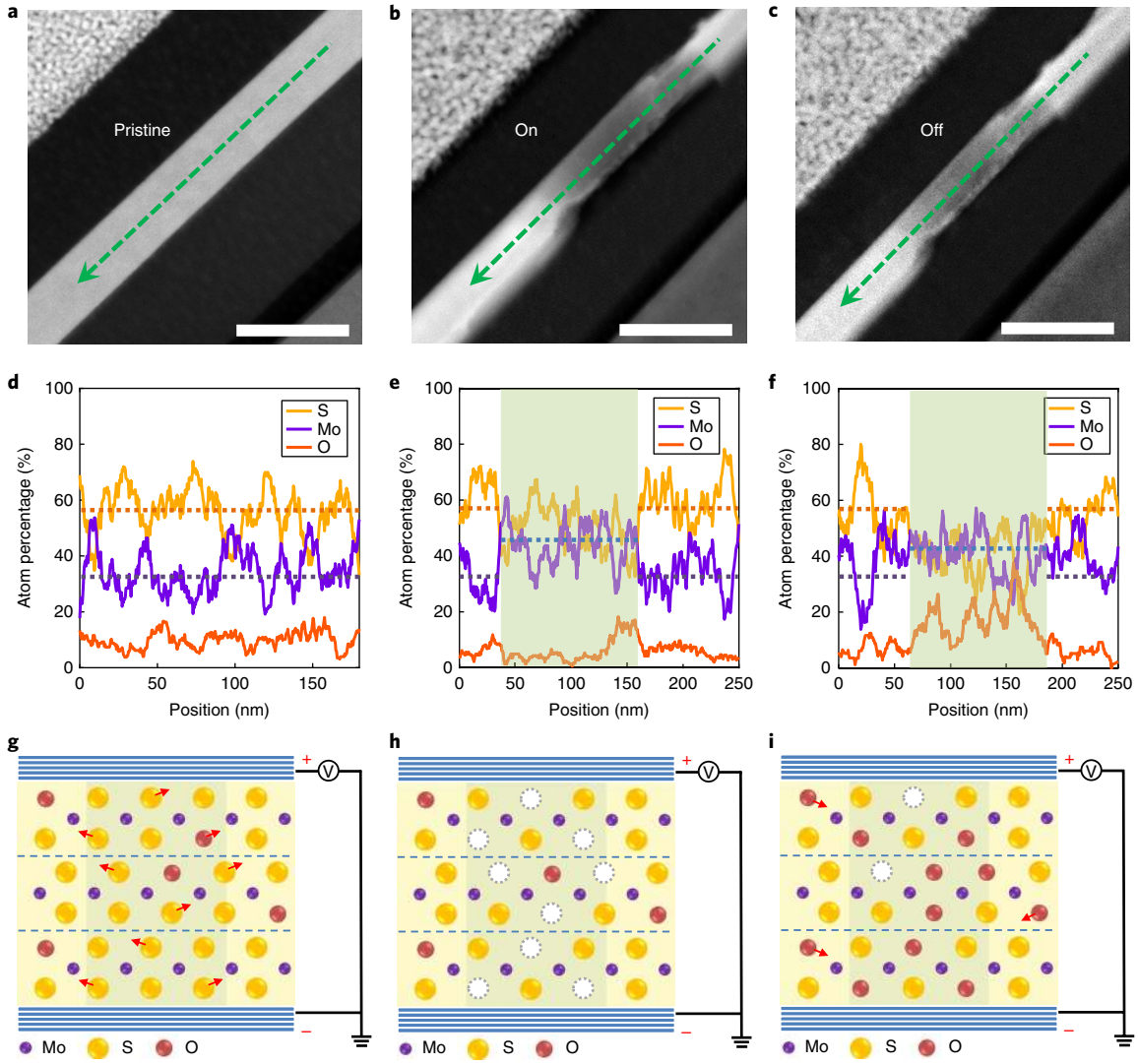

Fig. 5 | In situ STEM observation of the conduction channel in GMG devices. a–c, Cross-section HAADF image of a single GMG device in the pristine state (**a**), ON state (**b**) and OFF state (**c**). A dark region in the $MoS_{2-x}O_x$ layer appears in the ON state (**b**) and remains unchanged when the device is switched to the OFF state (**c**). All scale bars, 50 nm. **d–f**, EDS line-scan profiles of the green arrows in **a**, **b** and **c**, respectively. The numbers of Mo, S and O were measured and normalized as atom percentage. **d**, $MoS_{2-x}O_x$ layer in the pristine state shows a uniform atom distribution, where Mo:(S + O) ≈ 1:2. **e**, A reduction of S atoms was observed in the dark region, where Mo:(S + O) is approximately 1:1.2. **f**, An increase of O atoms was observed in the conduction channel for the OFF state, yielding a ratio of Mo:(S + O) back to the value near 1:2. **g–i**, Schematic structure diagrams illustrating resistance-switching mechanism in the GMG devices. **g**, Electroforming (from the pristine state) step, showing a uniform elemental distribution in the pristine state and the appearance of sulfur vacancies during electroforming. **h**, ON state with sulfur vacancies formed within the channel region. **i**, OFF state showing that the sulfur vacancies are filled with oxygen ions from the regions surrounding the channel.

ing regions. Secondly, with a high thermal and chemical stability[33] and good impermeability[52], the graphene electrodes act as protector of the conduction channel at elevated temperatures. Indeed, we noticed that the graphene electrodes maintain excellent crystal structure after switching (Supplementary Fig. 7b). The carbon EDS mapping of the channel region in pristine, ON and OFF states (Supplementary Fig. 8) further demonstrates the compositional stability of the graphene electrodes. With the help of the atomically sharp interface between graphene and $MoS_{2-x}O_x$ layer, the graphene electrodes well confine a stable conduction channel and effectively prevent the migration of the active ions[43] into electrode materials, which is strongly correlated to device failure, especially at elevated temperatures. This also explains in ambient conditions (with the existence of oxygen and humidity), the as-prepared MoS_2 membrane with existing sulfur vacancies[53] can be oxidized at quite low temperature (160 °C) to be $MoS_{2-x}O_x$, which still maintains good layered crystal structure (Fig. 1d). Nevertheless, after being isolated from oxygen and humidity (either in HRTEM vacuum or being well-protected by graphene electrodes), the $MoS_{2-x}O_x$ membrane has shown good structure stability at temperatures up to 800 °C in HRTEM (Fig. 4) and good electrical switching behaviors at temperatures up to 340 °C (Fig. 3).

Flexible electronic applications

Both graphene and MoS_2 have shown outstanding mechanical flexibility[34,54], which is ideal for harsh electronics against mechanical stress and other flexible electronic applications[40,55]. As a demonstration, we fabricated flexible GMG crossbar structures on PI substrate (Fig. 6a,b). The flexible GMG devices could be set at about 0.4 V with a current compliance of 1 mA, and reset at about −0.5 V (with switching curves of a typical device shown in Fig. 6c), which is comparable to the GMG devices on a SiO_2/Si substrate. As shown in

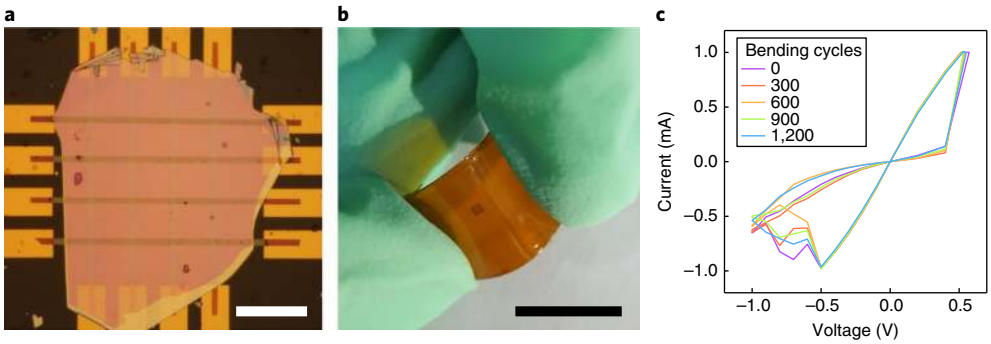

Fig. 6 | Flexible GMG devices. a, Optical microscope image of a GMG crossbar device on a PI substrate. Scale bar, 20 μm. **b**, A photograph of a crossbar array under bending. Scale bar, 10 mm. **c**, Switching curves of a GMG device against repeated mechanical bending to a 1-cm radius curvature.

Fig. 6c, the device exhibits excellent mechanical durability by maintaining critical resistance states and remaining functional over 1,000 bending cycles (corresponding to a strain of ~0.6%). Usually it is very challenging for electronic devices to possess both good flexibility and high thermal stability: inorganic material based devices usually lack mechanical flexibility while organic material based devices usually lack good thermal stability.

Conclusions

We fabricated robust memristors based on fully layered 2D materials (graphene/$MoS_{2-x}O_x$/graphene), which exhibit repeatable bipolar resistive switching and high thermal stability up to 340 °C. We found the atomically sharp interface formed between graphene and $MoS_{2-x}O_x$ is responsible for the observed high switching performance. $MoS_{2-x}O_x$ layer was found to induce the observed high thermal stability after performing high temperature in situ HRTEM studies. Further in situ STEM investigations on a cross-sectional device revealed a well-confined conduction channel and a switching mechanism based on the migration of oxygen ions. The atomic layered structure of both switching layer ($MoS_{2-x}O_x$) and electrodes (graphene), together with their atomically sharp interfaces, were found to play a crucial role in determining the robustness of the devices. Finally, the mechanical flexibility of such structured devices was demonstrated by showing a good endurance against mechanical bending of over 1,000 times, suggesting possible flexible electronic applications. Our realization of robust memristors based on fully 2D materials provides an avenue for future electronics engineering using vdW heterostructures.

Methods

Device fabrication. The multi-layer graphene and MoS_2 membranes were obtained by using mechanical exfoliation method on 300-nm thick SiO_2 wafers, where commercial graphite and MoS_2 flakes were used as received (graphite from Kish Graphite; MoS_2 from SPI Supplies). The graphene ribbons were defined by standard e-beam lithography (EBL) method, followed by dry etching in an Inductively Coupled Plasma (ICP) system, where O_2 was used as etching gas. The thickness of graphene and MoS_2 membranes was identified by an atomic force microscopy (AFM). The oxidation of the MoS_2 membranes was performed in ambient air on a hot plate at 160 °C for 1.5 h, with subsequent rapid cooling. The graphene/$MoS_{2-x}O_x$/graphene (GMG) structure was stacked by using standard polyvinyl alcohol (PVA) transfer method[26]. The metal conductive layer (5 nm Ti/50 nm Au) was deposited through standard E-beam deposition process. To fabricate Au/$MoS_{2-x}O_x$/Au (AMA) devices, we first deposited an Au bottom electrode (40 nm thick, 1 μm wide) on a 300-nm thick SiO_2 wafer through standard EBL and E-beam deposition processes. A $MoS_{2-x}O_x$ membrane was then transferred onto the bottom electrode. An Au top electrode (40 nm thick, 1 μm wide) was finally deposited onto the $MoS_{2-x}O_x$ membrane perpendicular to the bottom electrode.

Characterizations. Current–voltage switching curves and resistance measurements were performed using an Agilent B1500A parameter analyzer. The high temperature electrical measurements of GMG and AMA devices were performed on a hot plate in ambient air. The temperatures of the devices were further confirmed by a Fluke non-contact infrared thermometer.

High temperature in situ HRTEM experiments. MoS_2 nanosheets were prepared by ultrasonic exfoliation using commercial MoS_2 bulk samples (SPI Supplies). The dispersion was then dropped onto a DENSsolution in situ heating chip. Before the in situ HRTEM experiments, sample was heated to 160 °C in ambient air and kept 1.5 h for thermal oxidation. HRTEM images were acquired by FEI Tecnai F20 at 200 KV. DENSsolution DH30 system was used for in situ heating experiments.

In situ cross-section STEM experiments. High quality Pt (conductive protection layer)/graphene/$MoS_{2-x}O_x$/graphene/Si (conductive silicon substrate) samples were manufactured on our home-made in-situ electrical chip (designed for DENSsolution DH30 holder) by a Helios 600i dual-beam FIB system. The cross-sectional lamellae were thinned down to approximate 100 nm at an accelerating voltage of 30 kV with 0.79 nA, followed by two steps of fine polish at 5 kV accelerating voltage with 0.12 nA and 2 kV accelerating voltage with a small current of 68 pA, respectively. The lamellae were fixed on two electrodes of the in situ electrical chip by Pt deposition in the FIB system. The STEM and HRTEM images were obtained on a FEI Titan Cubed G2 60–300 aberration corrected S/TEM. The operation voltage of 60 kV was used to reduce electron beam damage to graphene and $MoS_{2-x}O_x$. EDS analyses were carried out using Bruker SuperEDX four-detector system. Real-time electrical measurements of the in situ samples were performed using a Keithley 2636 A dual channel digital source meter unit connected with a DENSsolution double-tilt heating and biasing holder. In this experiment, thicker graphene membranes (> 50 nm) were used for both top and bottom electrodes to protect the $MoS_{2-x}O_x$ layer from being damaged by the high energy focused ion beam (Gallium ion), and to avoid the disturbance of the Si and Pt atoms during the switching process.

Data availability. The data that support the plots within this paper and other findings of this study are available from the corresponding author upon reasonable request.

Received: 19 September 2017; Accepted: 9 January 2018;
Published online: 5 February 2018

References

1. Chua, L. O. Memristor - Missing circuit element. *IEEE Trans. Circuit Theory* **18**, 507–519 (1971).
2. Strukov, D. B., Snider, G. S., Stewart, D. R. & Williams, R. S. The missing memristor found. *Nature* **453**, 80–83 (2008).
3. Yang, J. J. et al. Memristive switching mechanism for metal/oxide/metal nanodevices. *Nat. Nanotech.* **3**, 429–433 (2008).
4. Waser, R. & Aono, M. Nanoionics-based resistive switching memories. *Nat. Mater.* **6**, 833–840 (2007).
5. Wong, H. S. P. et al. Metal-oxide RRAM. *Proc. IEEE* **100**, 1951–1970 (2012).
6. Yang, J. J., Strukov, D. B. & Stewart, D. R. Memristive devices for computing. *Nat. Nanotech.* **8**, 13–24 (2013).
7. Jo, S. H. et al. Nanoscale memristor device as synapse in neuromorphic systems. *Nano Lett.* **10**, 1297–1301 (2010).
8. Tuma, T., Pantazi, A., Le Gallo, M., Sebastian, A. & Eleftheriou, E. Stochastic phase-change neurons. *Nat. Nanotech.* **11**, 693–699 (2016).
9. Prezioso, M. et al. Training andoperation of an integrated neuromorphic network based on metal-oxide memristors. *Nature* **521**, 61–64 (2015).
10. Wang, Z. et al. Memristors with diffusive dynamics as synaptic emulators for neuromorphic computing. *Nat. Mater.* **16**, 101–108 (2017).

11. Kozicki, M. N., Park, M. & Mitkova, M. Nanoscale memory elements based on solid-state electrolytes. *IEEE Trans. Nanotechnol.* **4**, 331–338 (2005).
12. Szot, K., Speier, W., Bihlmayer, G. & Waser, R. Switching the electrical resistance of individual dislocations in single-crystalline $SrTiO_3$. *Nat. Mater.* **5**, 312–320 (2006).
13. Terabe, K., Hasegawa, T., Nakayama, T. & Aono, M. Quantized conductance atomic switch. *Nature* **433**, 47–50 (2005).
14. Rozenberg, M. J., Inoue, I. H. & Sanchez, M. J. Nonvolatile memory with multilevel switching: A basic model. *Phys. Rev. Lett.* **92**, 178302 (2004).
15. Lee, M. et al. A fast, high-endurance and scalable non-volatile memory device made from asymmetric Ta_2O_{5-x}/TaO_{2-x} bilayer structures. *Nat. Mater.* **10**, 625–630 (2011).
16. Miao, F. et al. Anatomy of a nanoscale conduction channel reveals the mechanism of a high-performance memristor. *Adv. Mater.* **23**, 5633–5640 (2011).
17. Kwon, D. et al. Atomic structure of conducting nanofilaments in TiO_2 resistive switching memory. *Nat. Nanotech.* **5**, 148–153 (2010).
18. Chen, C., Song, C., Yang, J., Zeng, F. & Pan, F. Oxygen migration induced resistive switching effect and its thermal stability in $W/TaO_x/Pt$ structure. *Appl. Phys. Lett.* **100**, 253509 (2012).
19. Lee, H. Y. et al. Low power and high speed bipolar switching with a thin reactive Ti buffer layer in robust HfO_2 based RRAM. *2008 IEEE Int. Electron Dev. Meeting* https://doi.org/10.1109/IEDM.2008.4796677 (2008).
20. Rahman, A. et al. A family of CMOS analog and mixed signal circuits in SiC for high temperature electronics. *2015 IEEE Aerospace Conf.* https://doi.org/10.1109/AERO.2015.7119302 (2015).
21. Herfurth, P. et al. GaN-on-insulator technology for high-temperature electronics beyond 400 degrees C. *Semicond. Sci. Tech.* **28**, 0740267 (2013).
22. Britnell, L. et al. Field-effect tunneling transistor based on vertical graphene heterostructures. *Science* **335**, 947–950 (2012).
23. Chae, S. H. et al. Transferred wrinkled Al_2O_3 for highly stretchable and transparent graphene-carbon nanotube transistors. *Nat. Mater.* **12**, 403–409 (2013).
24. Yu, W. J. et al. Highly efficient gate-tunable photocurrent generation in vertical heterostructures of layered materials. *Nat. Nanotech.* **8**, 952–958 (2013).
25. Britnell, L. et al. Strong Light-Matter Interactions in Heterostructures of Atomically Thin Films. *Science* **340**, 1311–1314 (2013).
26. Long, M. et al. Broadband photovoltaic detectors based on an atomically thin heterostructure. *Nano Lett.* **16**, 2254–2259 (2016).
27. Long, M. et al. Room temperature high-detectivity mid-infrared photodetectors based on black arsenic phosphorus. *Sci. Adv.* **3**, e1700589 (2017).
28. Xia, F., Wang, H., Xiao, D., Dubey, M. & Ramasubramaniam, A. Two-dimensional material nanophotonics. *Nat. Photon.* **8**, 899–907 (2014).
29. Liu, Y. et al. Van der Waals heterostructures and devices. *Nat. Rev. Mater.* **1**, 16042 (2016).
30. Geim, A. K. & Grigorieva, I. V. Van der Waals heterostructures. *Nature* **499**, 419–425 (2013).
31. Sahin, H. et al. Monolayer honeycomb structures of group-IV elements and III-V binary compounds: First-principles calculations. *Phys. Rev. B* **80**, 155453 (2009).
32. Miro, P., Audiffred, M. & Heine, T. An atlas of two-dimensional materials. *Chem. Soc. Rev.* **43**, 6537–6554 (2014).
33. Geim, A. K. Graphene: status and prospects. *Science* **324**, 1530–1534 (2009).
34. Bertolazzi, S., Brivio, J. & Kis, A. Stretching and breaking of ultrathin MoS_2. *ACS Nano* **5**, 9703–9709 (2011).
35. Tan, C., Liu, Z., Huang, W. & Zhang, H. Non-volatile resistive memory devices based on solution-processed ultrathin two-dimensional nanomaterials. *Chem. Soc. Rev.* **44**, 2615–2628 (2015).
36. Bessonov, A. A. et al. Layered memristive and memcapacitive switches for printable electronics. *Nat. Mater.* **14**, 199–204 (2015).
37. Son, D. et al. Colloidal synthesis of uniform-sized molybdenum disulfide nanosheets for wafer-scale flexible nonvolatile memory. *Adv. Mater.* **28**, 9326–9332 (2016).
38. Pan, C. et al. Coexistence of grain-boundaries-assisted bipolar and threshold resistive switching in multilayer hexagonal boron nitride. *Adv. Funct. Mater.* **27**, 1604811 (2017).
39. Sangwan, V. K. et al. Gate-tunable memristive phenomena mediated by grain boundaries in single-layer MoS_2. *Nat. Nanotech.* **10**, 403–406 (2015).
40. Yao, J. et al. Highly transparent nonvolatile resistive memory devices from silicon oxide and graphene. *Nat. Commun.* **3**, 1101 (2012).
41. Yang, Y. et al. Oxide resistive memory with functionalized graphene as built-in selector element. *Adv. Mater.* **26**, 3693–3699 (2014).
42. Cheng, P., Sun, K. & Hu, Y. H. Memristive behavior and ideal memristor of 1T phase MoS_2 nanosheets. *Nano Lett.* **16**, 572–576 (2016).
43. Liu, S. et al. Eliminating negative-SET behavior by suppressing nanofilament overgrowth in cation-based memory. *Adv. Mater.* **28**, 10623–10629 (2016).
44. Qian, M. et al. Tunable, ultralow-power switching in memristive devices enabled by a heterogeneous graphene-oxide interface. *Adv. Mater.* **26**, 3275–3281 (2014).
45. Molina, J. et al. Influence of the surface roughness of the bottom electrode on the resistive-switching characteristics of $Al/Al_2O_3/Al$ and $Al/Al_2O_3/W$ structures fabricated on glass at 300 degrees C. *Microelectron. Reliab.* **54**, 2747–2753 (2014).
46. Winer, W. O. Molybdenum disulfide as a lubricant - A review of fundamental knowledge. *Wear* **10**, 422–450 (1967).
47. Martin, N., Rousselot, C., Rondot, D., Palmino, F. & Mercier, R. Microstructure modification of amorphous titanium oxide thin films during annealing treatment. *Thin Solid Films* **300**, 113–121 (1997).
48. Chiu, F. C., Wang, J. J., Lee, J. Y. & Wu, S. C. Leakage currents in amorphous Ta_2O_5 thin films. *J. Appl. Phys.* **81**, 6911–6915 (1997).
49. Pennycook, S. J. & Jesson, D. E. High-resolution Z-contrast imaging of crystals. *Ultramicroscopy* **37**, 14–38 (1991).
50. Goldhirsch, I. & Ronis, D. Theory of thermophoresis. I. General considerations and mode-coupling analysis. *Phys. Rev. A* **27**, 1616–1634 (1983).
51. Kempers, L. A comprehensive thermodynamic theory of the Soret effect in a multicomponent gas, liquid, or solid. *J. Chem. Phys.* **115**, 6330–6341 (2001).
52. Bunch, J. S. et al. Impermeable atomic membranes from graphene sheets. *Nano Lett.* **8**, 2458–2462 (2008).
53. Qiu, H. et al. Hopping transport through defect-induced localized states in molybdenum disulphide. *Nat. Commun.* **4**, 2642 (2013).
54. Lee, C., Wei, X., Kysar, J. W. & Hone, J. Measurement of the elastic properties and intrinsic strength of monolayer graphene. *Science* **321**, 385–388 (2008).
55. Lee, G. et al. Flexible and transparent MoS_2 field-effect transistors on hexagonal boron nitride-graphene heterostructures. *ACS Nano* **7**, 7931–7936 (2013).

Acknowledgements

This work was supported in part by the National Key Basic Research Program of China (2015CB921600, 2015CB654901 and 2013CBA01603), National Natural Science Foundation of China (61625402, 61574076, 11474147 and 11374142), Natural Science Foundation of Jiangsu Province (BK20140017 and BK20150055), Fundamental Research Funds for the Central Universities, and Collaborative Innovation Center of Advanced Microstructures. Y.Z and J.J.Y. was supported in part by the U.S. Air Force Research Laboratory (AFRL) (Grant No. FA8750-15-2-0044) and DARPA (Contract No. D17PC00304).

Author contributions

F.M. and M.W. conceived the project and designed the experiments. M.W., C.P., C.W., X.L. and K.X. performed the device fabrication and electrical measurements. S.C., M.W. and P.W. carried out the in situ HRTEM and cross-section STEM experiments and analyses. M.W., F.M., X.L., T.C., Z.Y. and J.J. Yang conducted the data analyses and interpretations. F.M., M.W., S.C., S.L., P.W. and J.J. Yang co-wrote the paper, and all authors contributed to the discussions and preparation of the manuscript.

Competing interests

The authors declare no competing financial interests.

Additional information

Supplementary information accompanies this paper at https://doi.org/10.1038/s41928-018-0021-4.

Reprints and permissions information is available at www.nature.com/reprints.

Correspondence and requests for materials should be addressed to J.J.Y. or P.W. or F.M.

Publisher's note: Springer Nature remains neutral with regard to jurisdictional claims in published maps and institutional affiliations.